Soft Matter

Shock Compression of Semiflexible Polymers

Journal:	*Soft Matter*
Manuscript ID	SM-ART-06-2023-000765.R1
Article Type:	Paper
Date Submitted by the Author:	28-Jul-2023
Complete List of Authors:	Vega, Daniel; Universidad Nacional del Sur, Fisica del Sur Lance, Pedro; Universidad Nacional del Sur - IFISUR - CONICET, Physics Zorzi, Enzo; Universidad Nacional del Sur - IFISUR - CONICET, Physics Register, Richard; Princeton University, Chemical and Biological Engineering Gomez, L.; Universidad Nacional del Sur - IFISUR - CONICET, Physics

Soft Matter

ARTICLE TYPE

Cite this: DOI: 00.0000/xxxxxxxxxx

Shock Compression of Semiflexible Polymers

Daniel A. Vega,[a] Pedro Lance,[a] Enzo Zorzi,[a] Richard A. Register[b], and Leopoldo R. Gómez,*[a]

Received Date
Accepted Date

DOI: 00.0000/xxxxxxxxxx

We employ molecular dynamics simulations to investigate the shock compression of linear semiflexible polymers. While the propagation velocity of a shock primarily depends on density, both chain rigidity and chain orientation significantly influence the shock width and the final temperature of the system. In general, the shock wave triggers molecular buckling in chains oriented perpendicular to the compression front. Following the passage of the front, the semiflexible chains buckle with a wavelength that decreases with the compression speed as $\lambda_m \sim u_p^{-0.2}$, and subsequent relaxation leads to a banana-like liquid crystal phase. In ordered systems with molecules oriented perpendicular to the compression front, the shock width increases by a factor of up to 10 compared to a similar isotropic system, resulting in enhanced shock energy absorption. These findings indicate that chain stiffness plays a critical role in the impact absorption properties of polymeric materials.

1 Introduction.

Shocks and blast waves are extreme events which test the response of materials towards their limit of structural integrity. In general, the sudden increase of pressure due to the passage of a shock induces a strong non-linear behavior, which can even produce failure or fracture of the material [1–3]. Given its fundamental and technological relevance, there is a pressing interest in understanding the high-strain-rate response of different materials, such as metals, amorphous solids, ceramics, and polymers.

Their intrinsic rate-dependent behavior, light weight, tunable transparency, and self-healing ability, make polymers ideal materials for blast and impact absorption [4]. However, while the dynamic properties of most polymeric materials are now well-established at low deformation rates, much less is known about the mechanisms of mechanical response and energy dissipation at high deformation rates. A better understanding of the microscopic processes involved in impact absorption is fundamental for the design of novel polymeric systems with enhanced mechanical properties [5].

Indeed, some low-density polymeric materials show exceptional strength as compared with materials such as ceramics or metal alloys [6,7]. For example, multiphase polymeric elastomers like segmented poly(urethane urea)s have shown enormous capacity to absorb and dissipate energy while maintaining structural integrity [8,9]. In these polymeric systems, it is believed that their capacity for impact absorption comes from the combination of randomly distributed nanoscopic domains of soft and hard segments [7,10–12]. In this case, the soft domains are thought to be the main factor for impact dissipation, while the hard domains are expected to be a source of shock wave dispersion [6]. Applications include building and helmet coatings, reinforced structural composites, artificial joints for orthopedic devices, body armor, and coatings for satellite applications [6].

In anisotropic polymeric systems, such as aligned crystalline or stiff-chain polymers, deformation in the direction of the molecular axis requires a stretching or compression of chemical bonds. Thus, for polymers such as polyethylene, the elastic constant along the molecular axis can be up to 20 times higher than the constants in the other directions [13,14]. It is expected, then, that molecular orientation would play a key role in the non-linear response of polymers during the propagation of shocks and blast waves [15].

In this work we identify the main mechanisms of energy dissipation of shock waves in semiflexible polymer systems by means of molecular dynamics (MD) simulations (Fig. 1).

This work is organized as follows: In Section 2, we provide a concise review of the fundamental concepts and results of shock wave propagation in condensed matter systems. In Section 3, we outline the details of the coarse-grained molecular dynamics simulations conducted to examine shock compression in both ordered and disordered semi-flexible polymers. Section 4 presents the key findings of our study, including variations in velocity, width, temperature, and chain conformations, with respect to compression speed and chain stiffness, in both ordered and disordered systems. Finally, in Section 5, we summarize the main

[a] Department of Physics, Universidad Nacional del Sur - IFISUR - CONICET, 8000 Bahía Blanca, Argentina.
[b] Department of Chemical and Biological Engineering, Princeton University, Princeton, New Jersey, 08544, USA.

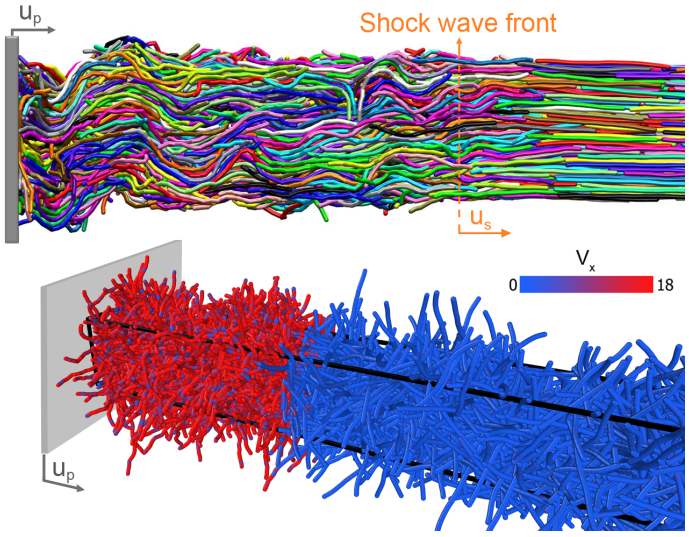

Fig. 1 Snapshots of the shock compression process for an ordered system (above) and a disordered system (below) are presented. In these examples, the compression and shock velocities are denoted as u_p and u_s, respectively. For the disordered system, beads are color-coded based on their respective velocities. For clarity, in the visual representations of chain configurations, we have unwrapped the periodic boundary conditions present in the directions orthogonal to u_p and u_s.

results obtained, and discuss the primary conclusions of our work.

2 Overview of Shock Wave Propagation in Condensed Matter

Shock waves are sudden disturbances that propagate through gases, liquids, or solids, resulting in rapid changes in pressure, density, and other material properties[1–3]. The study of shock waves has applications in different fields[6], such as aerospace, astrophysics, medicine, geophysics, and many others. In material science and polymers, shock waves can be used to study the behavior of materials under extreme conditions, such as high pressures and temperatures. This research can lead to the development of stronger, more resilient materials for various applications[1].

In a typical laboratory shock experiment, a medium is uniformly compressed at a high speed by a piston with velocity u_p. This compression generates a uniform shock wave that travels through the medium at an even higher velocity u_s. Under these conditions, the shock wave induces a rapid transition in the material's state. Since the transition between the initial and shocked states occurs quickly, the system lacks time for heat exchange, and the shock wave can be considered an adiabatic transition from a thermodynamic perspective.

Several key parameters describe the intensity of a shock wave and the material's response during the shock passage. Shock strength is typically characterized by the differences in pressure, density, and temperature between the initial and final states in the system. The greater these differences, the stronger the shock wave. Another common method to quantify shock strength is the Mach number (M), which represents the ratio of the shock wave's speed u_s to the local speed of sound c_0 in the undisturbed media. A shock wave with $M \gg 1$ is deemed a "strong" shock, while a shock with $M \gtrsim 1$ is commonly referred to as a "weak" shock.

A crucial parameter concerning shock wave passage is shock thickness (width), which provides a natural length scale and represents the spatial range over which physical properties (e.g., pressure, density, temperature) change. The shock wave width is influenced by the medium's properties and the shock strength, playing a role in how the shock's energy dissipates within the material. As shock width increases, the rate of energy dissipation generally increases due to molecular mechanisms and effects such as viscosity, thermal conduction, and radiation. For example, in the simplest case of shock waves traveling through monatomic gases, the shock thickness is approximately four mean free paths, meaning it takes about four molecular collisions to adjust the equilibrium state from upstream to downstream of the shock[3]. The molecular processes within the shock wave are not in equilibrium. Shock waves are wider in polyatomic gases because molecular rotation and vibration necessitate more collisions for equilibrium to be reached. Thus, molecular complexity and microscopic degrees of freedom can contribute to the enhancement of shock absorption and dissipation.

The behavior of shock waves can be better understood through the application of conservation laws, which dictate changes in physical properties across the shock interface[3]. These conservation laws are derived from the fundamental principles of mass, momentum, and energy conservation. For uniform shocks, the system can be described by an initial and shocked state, with variables changing exclusively across the shock interface. Under these circumstances, the conservation laws can be reformulated as the Rankine-Hugoniot jump conditions:

$$\begin{cases} \rho_0 u_s = \rho_s (u_s - u_p) \\ P_s - P_0 = \rho_0 u_s u_p \\ P_s u_p = \rho_0 u_s (1/2 u_p^2 + e_s - e_0) \end{cases} \quad (1)$$

Here, the indices 0 and s represent the values of density (ρ), pressure (P), and internal energy (e) before and after the shock wave passage, respectively. These relationships are established within the reference frame of the shock front. In this frame, the shock is in a steady state, and the net flow of mass, momentum, and energy towards the shock must be zero[3].

The shock adiabat, or Hugoniot curve, is a common tool for analyzing the features of a compressed region resulting from shock waves. It represents the locus of final shocked states and is an adiabatic line in the pressure-volume (P-V) plane. The Hugoniot curve is particularly valuable for constructing a material's equation of state, as the shock compression process is adiabatic in nature. Consequently, shock compression experiments have been extensively employed for many years to investigate the equation of state for various materials at high pressures[1,3].

The shock Hugoniot can be derived either directly from simulations by examining the final shocked states or by employing the Rankine-Hugoniot jump conditions. These conditions relate the pressure and volume in the material with particle and front

velocities as follows:

$$\begin{cases} V/V_0 = 1 - u_p/u_s \\ P - P_0 = \rho_0 u_s u_p \end{cases} \quad (2)$$

Thus, knowing the front velocity as a function of particle velocity, $u_s = u_s(u_p)$, these relations become an implicit expression for the Hugoniot curve.

The shock impedance relationship is a widely observed association in a multitude of materials. It presents a linear approximation between the shock speed (u_s) and particle velocity (u_p) as demonstrated by the following equation:

$$u_s = c + S u_p \quad (3)$$

Within this formula, c symbolizes the bulk sound speed in the undisturbed material, while S is a dimensionless constant referred to as the shock impedance or the slope of the Hugoniot curve. This linear approximation is generally well-suited for weak shocks. However, its accuracy can deviate for stronger shocks due to nonlinear effects.

There has been extensive research in recent years on the propagation of shock waves through polymeric systems. This has involved investigating the shock response of a wide variety of polymer classes, including glassy amorphous, semicrystalline, rubbery, and associative polymers, through both laboratory experiments and molecular dynamic simulations. A linear correlation between compression and shock velocity, as illustrated in Eq 3, was found to be applicable at low to moderate compression velocities for various systems such as polyethylene, epoxy, polycarbonate, polyimide, polysulfone, poly(tetrafluoroethylene), poly(methylmethacrylate), poly(vinylchloride), polybutadiene, polypropylene, and others[4,16–22]. Generally, at higher compression speeds, a deviation from linearity is observed in most systems. This can be attributed, among other factors, to pressure-induced breaking and re-formation of covalent bonds[23]. Using molecular dynamics simulations the shock response of several systems were analyzed, including segmented polyureas and polyurethanes[11,24–26], crystalline polymers[15,27,28], block copolymers[11,12], and amorphous systems[29–33].

In the present study, we focus on the shock compression of semiflexible chains, a topic that remains relatively under-researched compared to other polymer systems. We demonstrate that when semiflexible chains are aligned in the compression direction, the system responds to shock compression through a collective buckling of chains, where the dominant mode diminishes when increasing the compression velocity.

3 Simulation methods

Given the time and length scales needed to simulate these highly non-linear processes, coarse-grained molecular dynamics (CG-MD) can probe the microscopic relaxational mechanisms involved in these extreme stress-strain events. CG-MD has proven to be a key technique in the study of shock wave propagation in different solid materials[34], including polymers[25,35]. Here, CG-MD simulations were carried out with LAMMPS[36] using the Kremer-Grest (KG) standard polymer model[37]. The interaction between all

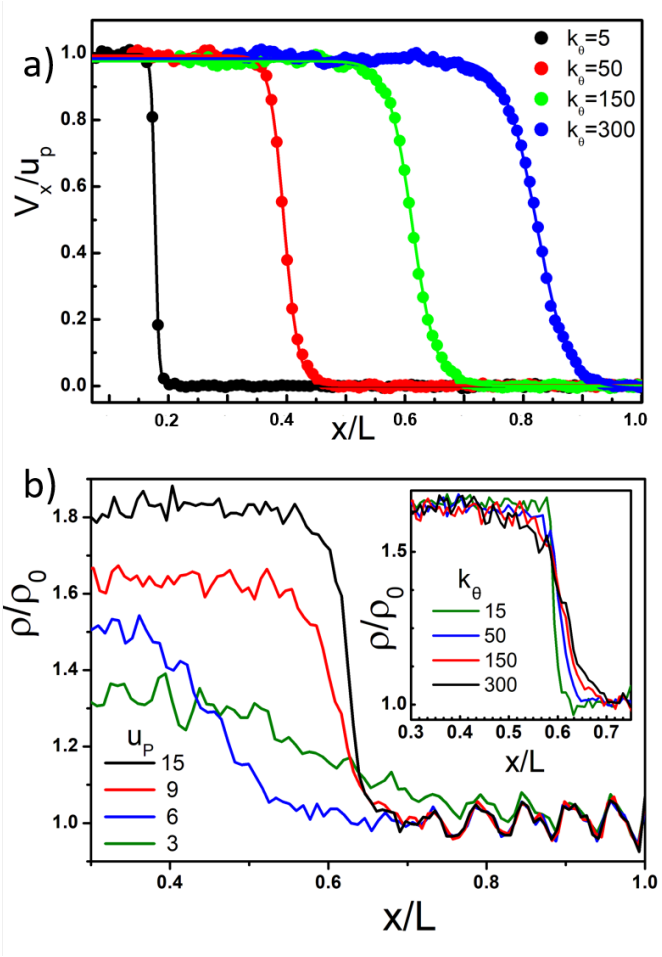

Fig. 2 Shock wave profiles as seen through the x-component of the particle velocity (a), and density ρ (b). The profiles are normalized with the piston compression velocity u_p, and initial density in the system ρ_0, respectively. The inset highlights that bending stiffness does not impact the final density, illustrated with $u_p = 9$ in this particular case.

beads was given by a purely repulsive Weeks-Chandler-Andersen (WCA) potential:

$$U_{WCA}(r) = 4\varepsilon[(\sigma/r)^{12} - (\sigma/r)^6] + \varepsilon \quad (4)$$

with $\varepsilon = 1$, $\sigma = 1$ and a cutoff of $r_c = 2^{1/6}\sigma$. In order to avoid bond crossing, chain breaking, and excessive bond stretching, bonded beads were coupled through a finitely extensible nonlinear elastic (FENE) potential:

$$U_{FENE}(r) = -k_F r_0^2 \ln[1 - (r/r_0)^2] \quad (5)$$

for $r < r_0 = 1.5\sigma$ and $k_F = 30\varepsilon/\sigma^2$.

The standard Kremer-Grest model was augmented with a harmonic bending potential:

$$U(\theta) = k_\theta(\theta - \theta_0)^2 \quad (6)$$

with $\theta_0 = \pi$ and k_θ between 15ε and 300ε, allowing the description of semi-flexible to rod-like molecules.

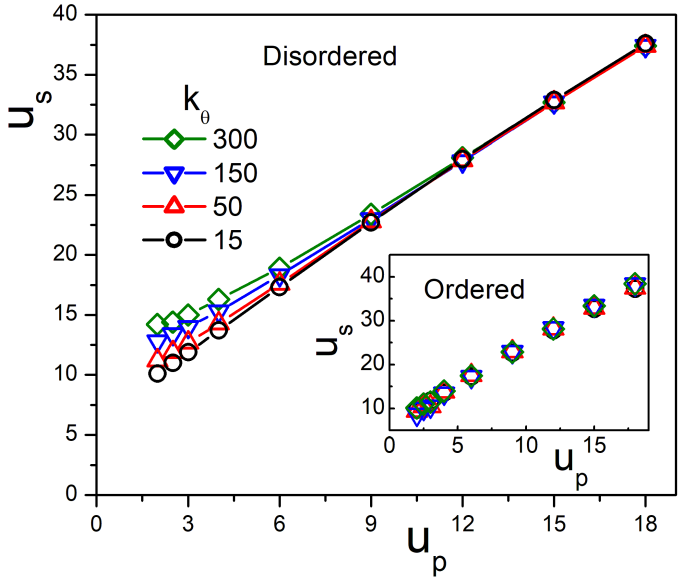

Fig. 3 Shock wave speed u_s versus piston speed u_p for disordered and ordered (inset) systems having different bending potential constants k_θ.

We simulate the propagation of shocks through semi-flexible polymers using systems with a particle density of $\rho = 0.84/\sigma^3$, consisting of 5,000 chains with 20 beads each.

To construct the initial configurations, chains were assembled using a random walk algorithm and subsequently placed randomly in a simulation box with periodic boundary conditions. The random walk chains were initially relaxed using dissipative particle dynamics (DPD), in which a soft potential facilitates rapid equilibration of the structure. The DPD potential was then replaced with a Lennard-Jones U_{WCA} potential[38]. Further relaxation of the melt involved NPT simulations, where the temperature and pressure were set at $T = k_B/\varepsilon$ and $P = 0.1\sigma^3/\varepsilon$, respectively. Here, the intrinsic MD time unit is $\tau_{MD} = \sqrt{m\sigma^2/\varepsilon}$, with $m = 1$ representing the mass of the monomers. This model results in an effective bond length of $l_b \sim 0.97\sigma$. The system dimensions' ratio after relaxation was $20:1:1$, yielding a size of approximately 20 stretched chains along the compression x-axis. Here all physical quantities are expressed in MD units; for example, u_p and u_s are in units of σ/τ_{MD}.

In ordered systems, alignment was induced in the initial configuration by using hard-wall boundary conditions, which was further relaxed through NPT simulations and periodic boundary conditions, as the temperature was insufficient to melt the quasi-crystalline order.

Upon obtaining the initial configuration, the periodic boundary conditions along the compression axis were removed (and the bonds of particles crossing those planes were eliminated). The shock wave was generated using a piston compression simulation in the NVE ensemble, where a wall compressed the box at a constant velocity u_p via the open-source software LAMMPS[39]. This process created a steep and narrow wavefront that traveled at a higher velocity u_s (Fig. 1)[40]. Due to the high piston velocity, a small time step of $\tau = 5 \cdot 10^{-6}$ was employed. During compression, the opposite face of the simulation box remained fixed.

4 Results

Figure 1 displays snapshots depicting polymer configurations during the shock compression of ordered (top) and disordered (bottom) semiflexible polymers. In the ordered system, all chains are aligned perpendicular to the direction of compression, resulting in a liquid-crystal-like structure. As noted in other systems[1,2], compression at a constant velocity (u_p) precipitates the formation of a shock front. Following an initial transient phase, this front progresses steadily at a superior, constant velocity (u_s). In this phase of steady propagation, the shock front traverses the system without undergoing any shape distortion. This allows us to pinpoint a well-defined shocked state where final particle velocity (u_p), pressure (P), and density (ρ) remain unchanged over time after the shock's passage.

Figure 2 provides a visual representation of the shock profiles in the compression direction (x) as seen through the x component of particle velocity (Fig. 2a) and local density (Fig. 2b). These shock profiles are derived by averaging the physical properties in the direction perpendicular to shock propagation. Analogous profiles can also be obtained using the local pressure or temperature of the systems.

Figure 2a clearly illustrates that during shock compression, following an initial transient phase and reaching a steady state, particles consistently move at the same speed as the piston. This behavior is observed irrespective of bond stiffness, compression velocity, system ordering, or initial density. Figure 2b reveals that the final density in the system after the shock wave passes depends on compression velocity but remains unaffected by bending stiffness (inset).

In general, shock propagation through condensed media can be examined by monitoring the motion and characteristics of the shock profiles. To better characterize the profiles of the shocks, we fit the velocity profiles using the expression[41]:

$$V_x = \frac{u_p}{2}\{1 + \tanh\left[\frac{2}{\Delta}(x_{front} - x)\right]\} \tag{7}$$

Here from the fits to the simulation data we can obtain the shock wave width Δ, and the position of the shock wave front x_{front}. Figure 2a demonstrates that this phenomenological fitting function (lines) accurately describes the velocity profiles.

By tracking the temporal evolution of the shock profile position (x_{front}), we can determine the shock propagation speed (u_s) under various conditions. Figure 3 displays the shock speed as a function of compression velocity for disordered systems with different bending constants. It is important to note that while the propagation velocity of strong shocks is similar across all systems, a higher bending constant increases the speed of sound c_0 in the system and the propagation velocity for weak shocks ($c_0 = u_s[u_p \to 0]$). In ordered systems, the shock speed is less sensitive to the bending constant (inset of Figure 3).

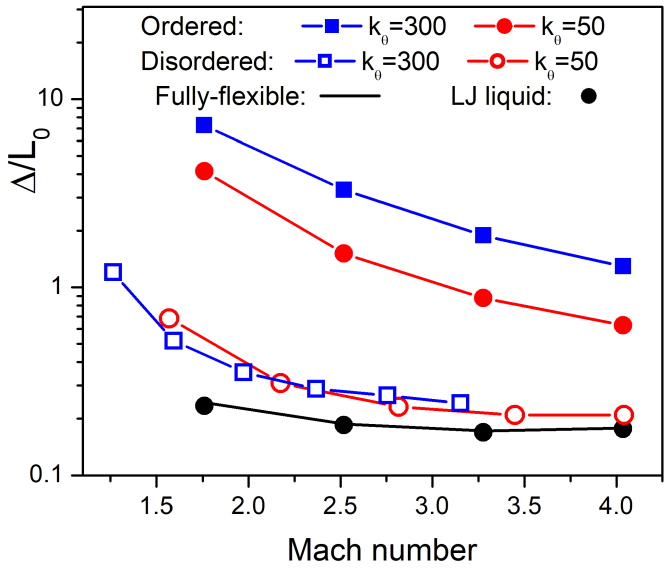

Fig. 4 Variation of the shock width with the Mach number for ordered and disordered systems of different bending constant k_θ (color symbols), and for a fully-flexible chain (black line), and a LJ fluid (black symnbols).

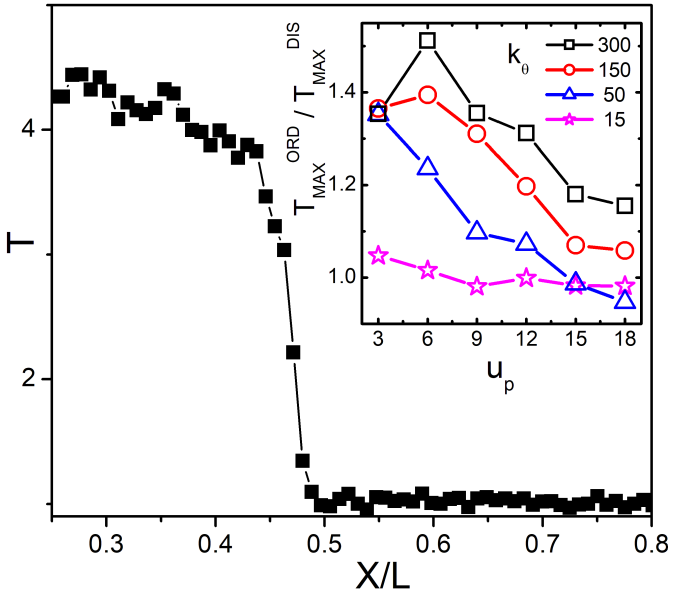

Fig. 5 A representative temperature profile, illustrating the effects of a passing shock wave, obtained by compressing a disordered system with $k_\theta = 150$ and at a velocity of $u_p = 6$. Inset: The final temperatures of compressed systems are consistently higher in ordered systems as compared to their disordered counterparts, regardless of the compression velocity and chain bending constant.

On the other hand, the bending constant significantly influences the shock's profile and width (Δ). As can be seen from Fig 2a, the propagation of shock waves along the chain axis of stiffer molecules generates gentler (wider) shock fronts.

Figure 4 depicts the shock's width Δ in units of the chain's extended end-to-end length (L_0), as a function of the Mach number $M = u_s/c$, where c is the speed of sound of the system. The speed of sound c is determined from Eq. 3 through a linear fit of u_s based on the data from Fig. 3, utilizing the four smallest compression velocities. This figure demonstrates that higher compression velocities produce shocks inducing faster transitions in the system (smaller Δ), as expected. For comparison purposes, this figure also includes the shock widths obtained for a purely repulsive Lennard-Jones fluid (WCA potential) at the same density. It is important to note that simulations for fully-flexible chains ($k_\theta = 0$) exhibited similar behavior to the purely-repulsive Lennard-Jones liquid. Consequently, control over intramolecular interaction potentials enables control over the energy density at the shock front.

Interestingly, Fig. 4 also clearly shows that shocks in ordered systems possess a significantly larger width (by a factor of 3-16), when compared to shocks in disordered systems. This finding suggests that the underlying molecular organization within a material greatly influences its shock response. As commented in section 2, the width of shocks is a critical parameter because it represents the material's ability to relax under rapid compression and is related to the mechanisms of energy dissipation. As the shock width increases, the rate of energy dissipation by the medium increases, meaning that the material is better suited for impact absorption. Understanding these effects is crucial for the development of advanced materials with tailored mechanical properties, such as shock absorption and energy dissipation.

The enhancement of thermal energy in both ordered and disordered systems stems directly from the continuous compression of the system due to energy injection. This energy transfer leads to alterations in the temperature profile of the systems. Figure 5 displays a representative temperature profile of a shock wave, generated by compressing a disordered system with a bending constant, $k_\theta = 150$, at a compression velocity, $u_p = 6$.

The temperature profile offers valuable information on the spatial distribution of temperature within the system as the shock wave moves through it. The inset of Fig. 5 highlights the ratio between the maximum temperature of ordered T_{MAX}^{ORD} and disordered T_{MAX}^{DIS} systems for various compression velocities and bending constants. This comparison facilitates a more comprehensive understanding of the impact of the system's structural organization on the distribution and dissipation of thermal energy during shock wave propagation.

Interestingly, these results show that ordered systems experience a more significant increase in thermal energy compared to disordered systems. This observation is consistent with our earlier analysis of shock wave width, implying that ordered systems should dissipate shock waves more efficiently than disordered systems due to their inherent structural organization. As illustrated in Fig. 5, ordered systems can also more effectively capture the injected energy from the shock wave, resulting in a higher final temperature. This increased energy capture can be ascribed to the more regular arrangement of particles in ordered systems, which fosters a more efficient transfer of energy throughout the system during shock wave propagation.

To better understand the molecular mechanism leading to

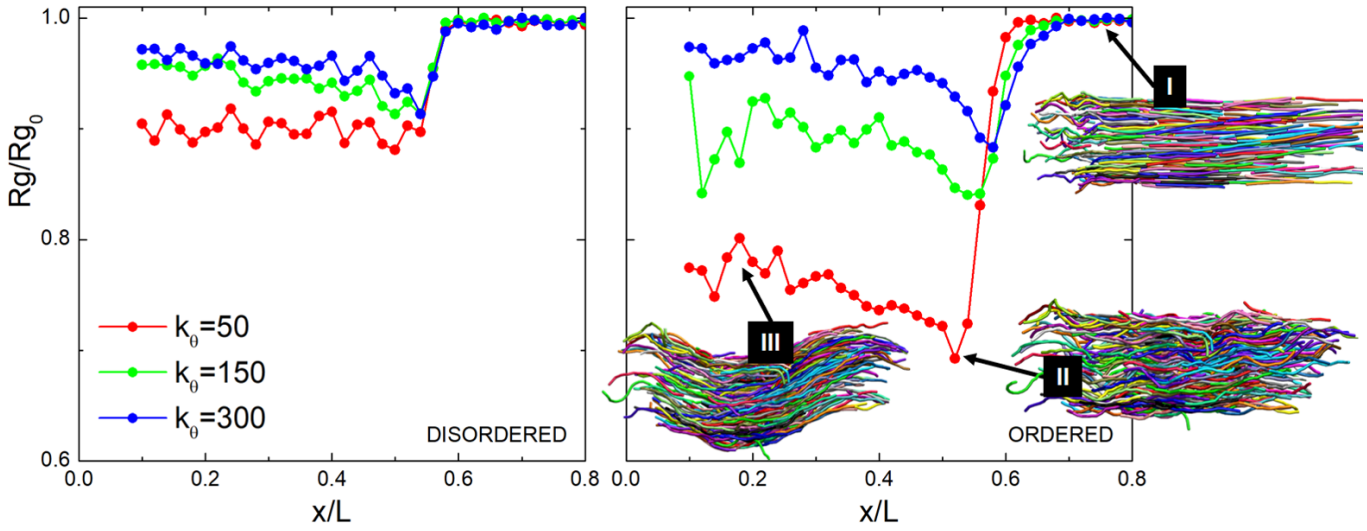

Fig. 6 Normalized radius of gyration profile along the x-axis for disordered (left) and ordered (right) systems with different bending constants. The insets show the dynamics of buckling in different regions; here, $u_p = 15$.

wider shocks for oriented chains, we study the chains' configurations during shock compression through the gyration tensor[42]:

$$S_{i,j} = 1/N_{beads} \sum_n [(r_{i,n} - r_{i,cm})(r_{j,n} - r_{j,cm})], \tag{8}$$

where the squared radius of gyration of the chains can be obtained from the eigenvalues β_i as $R_g^2 = Tr(S) = \beta_1 + \beta_2 + \beta_3$.

Figure 6 shows the temporal evolution of the mean radius of gyration, normalized by the initial value, for ordered and disordered systems. When the shock front arrives, the molecules rapidly contract, reducing their radius of gyration. While this occurs for both ordered and disordered systems, the contraction for ordered systems is larger. For the disordered systems, we find that for molecules oriented parallel to the shock direction, R_g suffers only minor changes while there is a clear reduction in R_g for those chains that were oriented perpendicular to the shock direction. This Figure also shows typical chain configurations during the shock compression for ordered systems. In this system, the initially ordered configuration (I) is distorted as the shock front arrives since chains rapidly contract by a buckling process (II). As time proceeds, the system relaxes and the buckled chains evolve towards a collective Euler-like buckled configuration (III) where the molecules self-assemble in a buckled state in order to relax the bending energy U_θ while satisfying packing constraints. The shock-induced buckled conformation described here has also been anticipated in stiff biopolymers under thermal fluctuations[43].

Upon visually inspecting the conformation of the chain subsequent to the shock passage, it was discerned that the chains can potentially buckle in either direction orthogonal to the compression direction. This results in the formation of structures exhibiting a certain degree of helicity, as graphically represented in Fig. 7a-b. Notably, analogous helical buckling phenomena were recently observed in experiments involving single fibers subjected to a significant compressional flow[44].

To conduct a systematic assessment of the helicity presented by the buckled chains, the writhe (W_r) of the polymer chains was computed following the shock passage. The writhe gives a quantitative metric to gauge the extent of a curve's helicity within a three-dimensional space, by enumerating the "signed" quantity of self-crossings projected by the curve onto a planar surface. The writhe of the polymer's chain contour C can be acquired via the Gauss double integral along C as given by[45,46]:

$$W_r = \frac{1}{4\pi} \int_C \int_C \frac{(d\mathbf{r}_1 \times d\mathbf{r}_2) \cdot \mathbf{r}_{12}}{|\mathbf{r}_{12}|^3}, \tag{9}$$

where $\mathbf{r}_1$ and $\mathbf{r}_2$ refer to points along the curve, and $\mathbf{r}_{12} = \mathbf{r}_2 - \mathbf{r}_1$.

The final writhe of compressed chains, represented as a function of the compression velocity u_p, for systems with varied bending constants k_θ, is showcased in Fig. 7c. A noteworthy observation is that the writhe distribution is symmetrically situated around zero, implying that both negative and positive helical configurations are equally probable. As the compression velocity escalates, and as the chain's bending constant diminishes, the writhe distribution tends to broaden, signaling that chain configurations become progressively more helical. This is clearly observed in the inset of Fig. 7c, where the width of the distribution—when fitted with a Lorentzian distribution—is plotted as a function of compression velocity, across differing bending constants. It is vital to note that despite the change in distribution width, the peak of the distributions remains at zero writhe. This suggests that the configurations of compressed chains should be characterized as weakly helical. Such a finding contrasts with observations from DNA molecules[47] or biopolymers[48], where highly helical molecular configurations are typically observed.

Fig. 8a shows a snapshot of the system configurations in the shocked region. As explained above, the passage of the shock induces buckling in the stiff chains. As the leading front moves away, the chains start to relax collectively, evolving into a self-organized undulated buckled state, whose wavelength exceeds

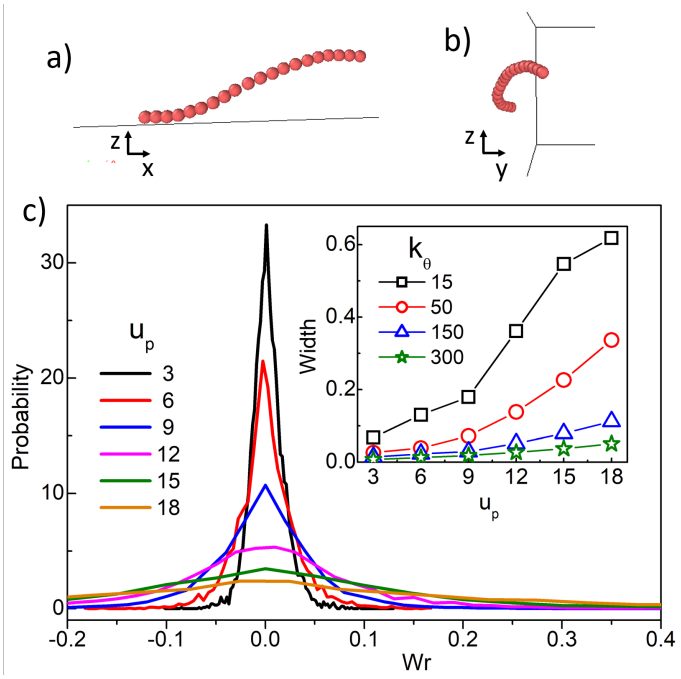

Fig. 7 a)-b) Weakly helical configuration of a compressed chain, as seen through the projection in the $x-z$ and $y-z$ planes. c) Writhe the probability distributions of a chain of bending constant $k_\theta = 150$, at different compression velocities. Inset: Width of the writhe distribution of compressed chains, as a function of compressing velocity, for different bending constants.

the length (L_0) of the individual chains.

To study the undulating buckled configurations, found as weakly helical, we first obtain the center of mass of the molecules along the compression direction (averaging in the $y-z$ plane), and then we Fourier transform its displacement to determine the leading length scales. Figure 8b shows the time evolution of the mode spectrum of buckled chain configurations induced by the passage of the shock through an ordered system. Note the presence of a leading mode at early times, induced by the buckled chains behind the shock front (see also Fig. 6). Interestingly, as the shock travels through the system, the wavelength of the leading mode remains nearly constant while the undulation amplitude increases over time due to the collective reorganization of the chains. The inset of Fig. 8b shows the dependence of the leading buckling wavelength λ_0 on the compression velocity. Larger compression velocities lead to stronger shocks and smaller wavelengths λ that scale as: $\lambda \sim u_p^{-0.2}$.

To elucidate the relationship between the primary buckling mode and the compression velocity, we employ the energy method conceptualized by Timoshenko and Gee, used for examining the buckling phenomenon in bars[49,50]. Within this context, the lateral deflection $v(x)$ of a buckled chain is characterized by the following Fourier series:

$$v(x) = \sum_{n=1}^{\infty} a_n \sin\left(\frac{n\pi x}{\lambda}\right) \tag{10}$$

The strain energy, arising from the bending of the chain, takes this form:

$$\Delta U = \frac{k_\theta}{2}\int_0^\lambda \frac{d^2v}{dx^2}, dx = \frac{\pi^4 k_\theta}{4\lambda^3}\sum_{n=1}^{\infty} n^4 a_n^2 \tag{11}$$

The work done by the piston, during the process of compressing the system, is represented as:

$$\Delta T = \frac{P_s \pi^2}{4\lambda}\sum_{n=1}^{\infty} n^2 a_n^2 \tag{12}$$

Thus, conservation of energy yields the following equation:

$$\frac{\pi^2 k_\theta}{\lambda^2}\sum_{n=1}^{\infty} n^4 a_n^2 = P_s \sum_{n=1}^{\infty} n^2 a_n^2 \tag{13}$$

It is important to emphasize that our system is undergoing shock compression. Through the use of an approximate Rankine-Hugoniot jump condition (Eq. 1) for the pressure $P_s \sim \rho_0 u_s, u_p$ (valid for $P_s \gg P_0$), and a linear Hugoniot relationship linking compression and shock velocities $u_s = c_0 + S u_p$ (Fig. 3), we can estimate $P_s \sim \rho_0 S u_p^2$. After incorporating these into our energy conservation equation (by only considering the leading mode), we derive an approximate connection between the primary buckling mode and the compression velocity:

$$\lambda \sim \sqrt{\frac{\pi^2 k_\theta}{\rho_0 S}}\, u_p^{-1/4} \tag{14}$$

This estimation aligns reasonably well with the exponent observed in the molecular dynamics simulations.

The buckling behavior of fibers or polymer chains under static compression has been a topic of rigorous study for years[43,50–54]. In static conditions, buckled states are determined by external load, chain size, bending constant, and temperature. Conversely, in our investigation of dynamic shock compression, we find that the buckling length is largely determined by compression velocity. Interestingly, similar power-law correlations between buckled length and compression rate have been identified in both experimental and theoretical studies, examining the conformations of individual fibers in a compression flow[44,55].

In addition to the leading mode, there is a longer-wavelength mode near $\lambda/L_0 \sim 7$ that increases over time, driven by the relaxation of the bending energy stored in the individual chains. Figure 8c shows the distribution of bending energy U_θ and the second Legendre polynomial P_2 along the shock direction. Here $P_2 = (3cos\Theta - 1)/2$, where Θ is the angle between a polymer bond and the director (direction of compression). A value of $P_2 = 1$ indicates parallel alignment, whereas a value of $P_2 = -1/2$ corresponds to a perpendicular orientation. For $P_2 = 0$, the bonds are oriented isotropically with respect to the director. Observe that U_θ shows a clear transition at the shock front, indicating the existence of buckled chains induced by the shock passage. In addition, P_2 reveals bond rotation in the shocked region, although a preferential direction still characterizes this zone.

At first sight this behavior is intriguing. Thermodynamically, a shock wave can be described as an adiabatic (irreversible) transition between two equilibrium states (initial and shocked)[1,2]. As

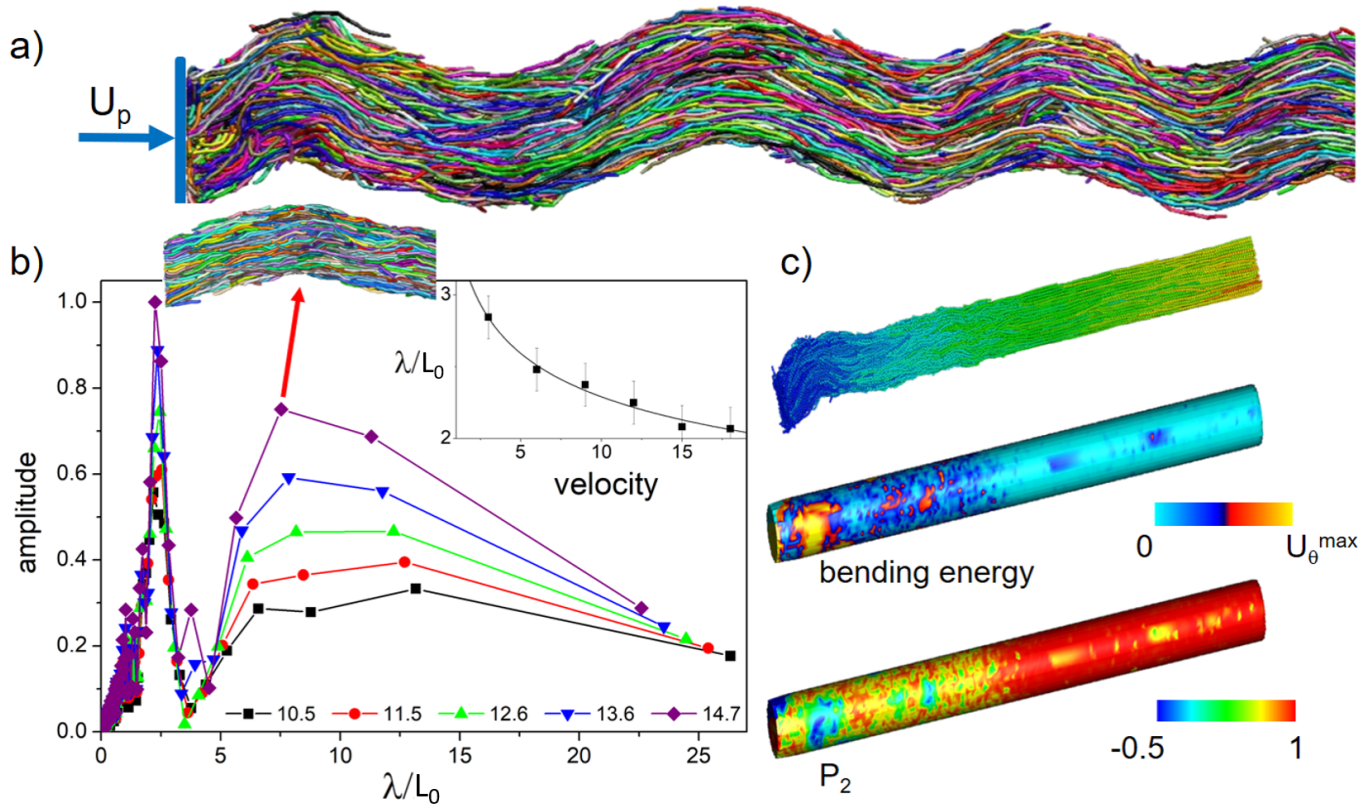

Fig. 8 a) Snapshot of the shock compression of an ordered system. Observe the collective organization of the buckled molecules. b) Temporal evolution of the spectrum of an ordered system with $k_\theta = 300$. Symbols denote different simulation times in units of τ_{MD}. Observe here a snapshot of chain conformation for the mode near $\lambda/L_0 \sim 7$. The inset shows that the leading wavelength decays with a power law with the compression velocity: $\lambda_m^* \sim u_p^{-0.2}$. c) This panel shows chain configuration (top), bending energy (middle), and P_2 (bottom) at an early stage of the buckling process.

pointed out above, here the Rankine-Hugoniot relations[1,2] connecting the states on both sides of a shock wave are satisfied. However, while the system studied here shows the typical features of a shocked state, in the sense that the particles have a clearly distinct density, velocity, and pressure profile along the shock, we found that this state is not well-defined in the classical sense, as here there is a slow relaxation in the shocked regions towards a banana-like liquid-crystal phase[56].

5 Conclusions

We have investigated the characteristics of shock compression in semiflexible polymers and demonstrated that the energy density distribution is influenced by both chain stiffness and orientation. During shock compression, chains generally reduce their radius of gyration along the compression direction. Chains oriented perpendicular to the shock front undergo a buckling process. This mechanism broadens the shock's width and is anticipated to be the primary dissipation process for shocks traversing systems with highly oriented molecules or fibers.

We observed a significant difference in the shock response of ordered and disordered systems. In ordered systems, chains are arranged in a regular pattern, facilitating a more synchronized response when subjected to stress. The buckling of multiple chains requires cooperative motion among several chains, with a single chain's ability to buckle and respond to stress depending on neighboring chains buckling in a similar manner. As a result, when chains in an ordered system experience stress, they are more likely to buckle collectively, allowing for a coordinated response. Conversely, isotropic systems exhibit a random arrangement of chains, which disrupts cooperative motion among chains and prevents them from buckling collectively. Consequently, chains in disordered systems cannot effectively respond to stress due to the lack of synchronized buckling in neighboring chains.

The collective buckling of chains in ordered systems leads to a larger distortion of the media, resulting in an increased shock width and temperature increase, which contributes to enhanced absorption of energy from the shock wave. This energy absorption reduces the shock's intensity as it propagates through the material, resulting in more effective shock attenuation. In contrast, the absence of collective buckling in disordered systems hinders their ability to absorb energy from the shock wave, leading to less effective shock attenuation.

Author Contributions

DAV and LRG designed research; EZ and PL performed the simulations; all the authors analyzed data and discussed the results; and all the authors wrote the paper.

Conflicts of interest

There are no conflicts to declare.

Acknowledgements

LRG acknowledges support from the Alexander von Humboldt Foundation through the Georg Forster and return fellowships. We acknowledge support from Universidad Nacional del Sur, the National Research Council of Argentina (CONICET), the Fondo para la Investigación Científica y Tecnológica (FONCYT, Grant PICT-2017-3611), the US Army RDECOM-Americas and US ARO (Grant Number W911NF-18-1-0401).

Notes and references

1 M. A. Meyers, *Dynamic behavior of materials*, John wiley & sons, 1994.

2 Y. B. Zel'Dovich and Y. P. Raizer, *Physics of shock waves and high-temperature hydrodynamic phenomena*, Courier Corporation, 2002.

3 G. Ben-Dor, O. Igra and T. Elperin, *Handbook of shock waves, three volume set*, Elsevier, 2000.

4 W. J. Carter and S. P. Marsh, *Hugoniot equation of state of polymers*, Los alamos national lab.(lanl), los alamos, nm (united states) technical report, 1995.

5 A. J. Hsieh, Y.-C. M. Wu, W. Hu, J. P. Mikhail, D. Veysset, S. E. Kooi, K. A. Nelson, G. C. Rutledge and T. M. Swager, *Polymer*, 2021, **218**, 123518.

6 R. G. S. Barsoum, *Elastomeric polymers with high rate sensitivity: applications in blast, shockwave, and penetration mechanics*, William Andrew, 2015.

7 J.-H. Lee, D. Veysset, J. P. Singer, M. Retsch, G. Saini, T. Pezeril, K. A. Nelson and E. L. Thomas, *Nature communications*, 2012, **3**, 1164.

8 D. Veysset, A. J. Hsieh, S. Kooi, A. A. Maznev, K. A. Masser and K. A. Nelson, *Scientific reports*, 2016, **6**, 25577.

9 D. Veysset, A. J. Hsieh, S. E. Kooi and K. A. Nelson, *Polymer*, 2017, **123**, 30–38.

10 J. Hyon, O. Lawal, O. Fried, R. Thevamaran, S. Yazdi, M. Zhou, D. Veysset, S. E. Kooi, Y. Jiao, M.-S. Hsiao *et al.*, *Materials Today*, 2018, **21**, 817–824.

11 B. Arman, A. S. Reddy and G. Arya, *Macromolecules*, 2012, **45**, 3247–3255.

12 L. Ortellado, D. A. Vega and L. R. Gómez, *Physical Review E*, 2022, **106**, 044502.

13 D. J. Pastine, *The Journal of Chemical Physics*, 1968, **49**, 3012–3022.

14 I. Satcurada, T. Ito and K. Nakamae, Journal of Polymer Science Part C: Polymer Symposia, 1967, pp. 75–91.

15 T. C. O'Connor, R. M. Elder, Y. R. Sliozberg, T. W. Sirk, J. W. Andzelm and M. O. Robbins, *Physical Review Materials*, 2018, **2**, 035601.

16 S. Walley and J. Field, *DYMAT j*, 1994, **1**, 211–227.

17 N. K. Bourne, *Journal of Dynamic Behavior of Materials*, 2016, **2**, 33–42.

18 J. Millett and N. Bourne, *Journal of Physics D: Applied Physics*, 2004, **37**, 2901.

19 J. Millett, N. Bourne and J. Akhavan, *Journal of applied physics*, 2004, **95**, 4722–4727.

20 J. Millett, E. Brown, G. Gray, N. K. Bourne, D. Wood and G. Appleby-Thomas, *Journal of Dynamic Behavior of Materials*, 2016, **2**, 326–336.

21 C. R. Siviour and J. L. Jordan, *Journal of Dynamic Behavior of Materials*, 2016, **2**, 15–32.

22 J. L. Jordan, D. T. Casem and J. Robinette, *Journal of Applied Physics*, 2022, **131**, 165903.

23 T. L. Chantawansri, T. W. Sirk, E. F. Byrd, J. W. Andzelm and B. M. Rice, *The Journal of chemical physics*, 2012, **137**, 204901.

24 M. Grujicic, B. Pandurangan, W. Bell, B. Cheeseman, C.-F. Yen and C. Randow, *Materials Science and Engineering: A*, 2011, **528**, 3799–3808.

25 F. Xie, Z. Lu, Z. Yang, W. Hu and Z. Yuan, *Polymer*, 2016, **98**, 294–304.

26 M. Manav and M. Ortiz, *Polymer*, 2021, **212**, 123109.

27 R. M. Elder, T. C. O'Connor, T. L. Chantawansri, Y. R. Sliozberg, T. W. Sirk, I.-C. Yeh, M. O. Robbins and J. W. Andzelm, *Physical Review Materials*, 2017, **1**, 043606.

28 M. Dewapriya and R. Miller, *Journal of Applied Physics*, 2022, **131**, 025102.

29 L. He, T. D. Sewell and D. L. Thompson, *Journal of Applied Physics*, 2013, **114**, 163517.

30 M. G. Fröhlich, T. D. Sewell and D. L. Thompson, *The Journal of Chemical Physics*, 2014, **140**, 024902.

31 L. Liao, X. Wang and C. Huang, *Modelling and Simulation in Materials Science and Engineering*, 2020, **29**, 015008.

32 M. Dewapriya and R. Miller, *Journal of Applied Mechanics*, 2021, **88**, year.

33 G. Lecoutre, C. A. Lemarchand, L. Soulard and N. Pineau, *Macromolecular Theory and Simulations*, 2021, **30**, 2000068.

34 L. Davison, *Fundamentals of shock wave propagation in solids*, Springer Science & Business Media, 2008.

35 Y. Fu and J.-H. Song, *Computational Materials Science*, 2015, **96**, 485–494.

36 S. Plimpton, *Computational Materials Science*, 1995, **4**, 361–364.

37 K. Kremer and G. S. Grest, *The Journal of Chemical Physics*, 1990, **92**, 5057–5086.

38 Y. R. Sliozberg and J. W. Andzelm, *Chemical Physics Letters*, 2012, **523**, 139–143.

39 A. P. Thompson, H. M. Aktulga, R. Berger, D. S. Bolintineanu, W. M. Brown, P. S. Crozier, P. J. in 't Veld, A. Kohlmeyer, S. G. Moore, T. D. Nguyen, R. Shan, M. J. Stevens, J. Tranchida, C. Trott and S. J. Plimpton, *Comp. Phys. Comm.*, 2022, **271**, 108171.

40 P. Wen, G. Tao, D. E. Spearot and S. R. Phillpot, *Journal of Applied Physics*, 2022, **131**, 051101.

41 L. R. Gómez, A. M. Turner and V. Vitelli, *Physical Review E*, 2012, **86**, 041302.

42 H. Arkın and W. Janke, *The Journal of chemical physics*, 2013, **138**, 054904.

43 M. Emanuel, H. Mohrbach, M. Sayar, H. Schiessel and I. M. Kulić, *Physical Review E*, 2007, **76**, 061907.

44 B. Chakrabarti, Y. Liu, J. LaGrone, R. Cortez, L. Fauci, O. Du Roure, D. Saintillan and A. Lindner, *Nature Physics*, 2020, **16**, 689–694.

45 E. Orlandini and S. G. Whittington, *Reviews of modern physics*, 2007, **79**, 611.

46 L. R. Gómez, N. A. García and T. Pöschel, *Proceedings of the National Academy of Sciences*, 2020, **117**, 3382–3387.

47 K. Klenin and J. Langowski, *Biopolymers: Original Research on Biomolecules*, 2000, **54**, 307–317.

48 Y. Jung and B.-Y. Ha, *Scientific reports*, 2019, **9**, 869.

49 S. P. Timoshenko and J. M. Gere, *Theory of elastic stability*, Courier Corporation, 2009.

50 S. J. DeTeresa, R. S. Porter and R. J. Farris, *Journal of materials science*, 1985, **20**, 1645–1659.

51 M. Dobb, D. Johnson and B. Saville, *Polymer*, 1981, **22**, 960–965.

52 N. Fleck, *Advances in applied mechanics*, 1997, **33**, 7.

53 T. Odijk, *The Journal of chemical physics*, 1998, **108**, 6923–6928.

54 J. Blundell and E. Terentjev, *Soft Matter*, 2009, **5**, 4015–4020.

55 J. Cappello, O. Du Roure, F. Gallaire, C. Duprat and A. Lindner, *Physical Review Letters*, 2022, **129**, 074504.

56 C. Fernández-Rico, M. Chiappini, T. Yanagishima, H. de Sousa, D. G. Aarts, M. Dijkstra and R. P. Dullens, *Science*, 2020, **369**, 950–955.